MANSOURA JOURNAL OF CHEMISTRY
Official Journal of Faculty of Science, Mansoura University, Egypt
E-mail: scimag@mans.edu.eg ISSN: 2974-4938

Isatin functionalized reduced graphene oxide for the simultaneous detection of heavy metals traces.

*Nada A. El-Amrity, Mina Shawky Adly, Ahmed Mosa, Amr Awad Ibrahim**

Chemistry department, Faculty of science, Mansoura University, Egypt)

**** Correspondence to:** na408726@gmail.com, 01068757371*

Received:18/7/2023
Accepted: 9/9/2023

Abstract: The simultaneous, sensitive, and convenient detection of many ions of heavy metal is a difficult challenge. The four primary heavy metal ion contaminants (Cu^{2+}, Hg^{2+}, Cd^{2+}, and Pb^{2+}) were detected simultaneously using a unique ratiometric electrochemical sensing approach developed in this article. The construction of platform sensor was applied by a chelating agent of Isatin (2,3-diketo derivative of indole) functionalized reduced graphene oxide (rGO). The as-fabricated catalyst (ISG) exhibited unique features including high porosity and a large surface area, both of which are advantageous for heavy metal ions for adsorption and preconcentration processes. The as-synthesized nanocomposites were analyzed by scanning electron microscopy (SEM, JEOL JSM 6510lv), the interfacial properties of the materials and their crystalline phase were examined. Moreover, Thermal gravimetric analysis was conducted using Shimadzu 50 under N_2 gas flow. The X-ray diffraction (XRD) patterns were carried out to characterize the crystal structure at 2θ range of 5°–70° by a Bruker device. Furthermore, FT-IR patterns were recorded for determination the functional groups in the structure (FT-DATR in wavenumber ranging from 500 to 4000 cm^{-}. Square wave anodic stripping voltammetry (SWASV), a technique utilized in the determination of metal ions, was used for investigation the electrochemical characteristics of the ISG. The modified electrode indicated enhanced excellent sensitivity and electrochemical catalytic activity towards trace ions of heavy metals. For determination of the target metal ions, several parameters, including time and potential preconcentration, were carefully optimized. For Hg^{2+}, Cd^{2+}, Cu^{2+}, and Pb^{2+}, the linear range of the electrode was 5-20 µM under optimized conditions, with low detection limits (LOD) of 1.35, 1.37, 1, and 0.5 µM, respectively.

keywords: graphene, heavy metal ion , isatin , electrochemical sensor

1.Introduction

Increased wastewater discharges including several heavy metal ions (HMIs), including Cu^{+2},Cd^{+2}, $Pb^{+2}$and Hg^{+2} is a result of rapid industrialization [1]. Most of these metal ions are extremely poisonous, nonbiodegradable, and bio accumulative. They will completely and irreparably harm human health once they enter the human body via the food chain. Due to this, even low quantities of some heavy metal ions can result in major health issues, such as those affecting the kidneys, liver, skin, bones, or teeth (Ni^{2+}, Cu^{2+}, Cd^{2+}, Cr^{2+}), the central nervous system (As^{3+},Hg^{2+}, Pb^{2+},), or the liver, kidneys, or other organs (Cu^{2+}, Hg^{2+},Cd^{2+}, , Pb^{2+}).Toxic heavy metal pollution has received a lot of attention worldwide. Although they can gradually accumulate throughout the food chain, heavy metals are quickly removed [2-5]. It is very important to develop heavy metal ion detection techniques with high sensitivity and reliability to prevent the harm that heavy metal ions can do to the environment and humanity. Considering that heavy metal ions typically coexist in multiples in pollution, it is essential that develop simultaneous detection techniques for various heavy metal ions. The mutual interference of heavy metal ions in solution, including the creation of competing and intermediate alloys on active sites, makes it difficult for

determination numerous ions at once [6]. Single-ion detection is the focus of most determination techniques. There is a significant practical need for the advancement of simultaneous determination technologies that are practical and reliable for numerous metal ions. Trace ions of heavy metal are currently detected using several analytical techniques, such as flame atomic absorption spectrometry (FAAS)[7], atomic absorption spectroscopy[8], and inductively coupled plasma mass spectrometry (ICP-MS)[9]. These procedures typically need expensive tools and analytical techniques carried out by trained professionals. A lot of work is being done to create a quick and easy method for finding small quantities of heavy metal.

So far, Atomic absorption/emission spectroscopy, hyper-Rayleigh scattering, inductively coupled plasma mass spectrometry, X-ray fluorescence spectrometry, inductively coupled plasma optical emission spectroscopy, electrochemical methods, and others have all been developed for detection the concentrations of heavy metal ions [10, 11]. The electrochemical approach has among them demonstrated great potential for on-site and real-time determine, as well as long-term research concern.[12]. It has portable instruments, easy monitors, quick responses, and excellent sensitivity. Additionally, the electrochemical detection approach provides special benefits for the simultaneous determination of several ions. As a result, significant effort should be put into developing electrochemical monitor methods for ions of heavy metal [13]. The advancement of electrochemical sensing is being pushed forward by the extraordinary advancements being made in the fields of nanotechnology and functional materials [14]. Materials that are functional can be utilized to make good electrochemical determination platforms for monitoring the ions in the environment due to their distinctive structural and physical properties [15]. The current frontier and focus of research on electrochemical sensors are creating electrodes with high performance modified with nano- or functional materials to increase the stability, selectivity, sensitivity, and electrochemical determination. Utilizing carbon compounds, such as carbon nanotubes and graphene, is a frequent strategy. Graphene, a planar sheet of sp^2 linked carbon atoms that is one atom thick, is also an innovative and exciting carbon material because of its distinct mechanical thermal and electrochemical characteristics. In addition, compared to other carbon-based materials, graphene has a greater specific surface area. This combination of physical characteristics makes graphene useful in a variety of technical domains, including nanoelectronics, capacitors, and sensors. Numerous groups have reported the combination of nanoparticles and graphene using a variety of techniques [16, 17]. Wide-ranging applications are made possible by their improved qualities, including as in energy storage, biological sectors, and catalysis [18]. Some heavy metals can bind to biological ligands that contain oxygen, nitrogen, and sulphur. improved graphene with Isatin (2,3-diketo derivative of indole) as chelator that contain nitrogen group a ratiometric Technique for electrochemical sensing for the simultaneous detection of Pb^{2+}, Hg^{2+}, Cu^{2+} and Cd^{2+} ions was developed. The modified graphene electrode showed a good electrochemical response to Hg^{2+}, Pb^{2+}, Cu^{2+} and Cd^{2+} with a linear range of 5-20 μM and low detection limits (LOD) of 1.35, 0.5, 1,1.37 and μM, respectively. As an electrochemical sensing platform for sensitive and focused monitoring of heavy metal ions, we developed a glassy carbon electrode (GCE). after characterizing the as-synthesized material and demonstrating the stable production of chelating agent on graphene. According to the results of the experiment, this electrode demonstrated improved electrochemical performance and greater sensitivity to heavy metal ions electrocatalytically. Finally, the concentrations of Cu^{2+}, Cd^{2+}, $Hg^{2+}$and Pb^{2+} were measured using this simple, inexpensive, and extremely sensitive sensor.

2. Materials and methods

2.1. Materials and chemicals

All chemicals utilized were obtained from commercial sources without additional purification. lead chloride ($PbCl_2$), cadmium chloride ($CdCl_2$), cupper chloride ($CuCl_2$), mercuric chloride ($HgCl_2$) and Isatin were obtained from Sigma Aldrich., Sodium Nitrate

($NaNO_3$), potassium permanganate ($KMnO_4$), and graphite were purchased from Alfa Aesar. Sulfuric acid (H_2SO_4), thionyl chloride, benzene, pyridine, and hydrogen peroxide (H_2O_2) were acquired from Merk. Sodium Acetate (CH3COONa) and Acetic acid (CH_3COOH) were used for the preparation of Acetate buffer. Deionized water (DI) (18 M cm) was obtained from the Millipore water system used to prepare all aqueous solutions.

2.2. Synthesis of Graphene Oxide (GO)

The high-purity graphite powder (99.95%) was utilized to produce GO sheets with modifications. Then add 115 mL of H_2SO_4 concentrated at 0 ºC (in an ice bath). After adding 2.5 g of ground NaNO3 to the initial solution, which had already contained 4.0 g of graphite powder, the NaNO3 was entirely dissolved. Then, 15.0 g of KMnO4 is slowly added to the mixture. After 15 min, 930 mL DI H2O was then added after the mixture had been heated to 35 ºC for three hours. After 20 minutes, 20 mL of 10% H2O2 was added to the mixture, and the color changed to golden yellow. The resultant graphene oxide was then washed with 2 L of (HNO3) and 5 L of hot DI H2O (80-100 ºC), 1 L each time, before being dried at 60 ºC.[19].

2.3. Synthesis of modified graphene.

A suspension of graphene oxide (0.5 g) in thionyl chloride (20 mL) was heated through reflux for 12 h. Next, thionyl chloride was eliminated while operated at lower pressure. and the obtained solid material was subjected to an *in-situ* reaction with hydrazine hydrate (10 mL) at 100 ^{o}C for 5 h. After that, the reaction mixture was filtered out. and the produced precipitate was washed several times with water to give the corresponding hydrazide derivative **1**.

To a suspension of **1** in ethanol, isatin (0.6 g) was added. At 80˚C, the reaction mixture was stirred. for 8 h till the complete consumption of isatin. The finished solid structure was then filtered off, washed by water, and dried to give the corresponding modified graphene oxide.

2.4. Material Characterization

Multiple analysis techniques were used to confirm the successful preparation. Using EDX methods and scanning electron microscopy (SEM, JEOL JSM 6510lv), the interfacial properties of the materials and their crystalline phase were examined. Moreover, Thermal gravimetric analysis was conducted using Shimadzu 50 under N_2 gas flow. The X-ray diffraction (XRD) patterns were carried out to characterize the crystal structure at 2θ range of 5°–70° by a Bruker device (λ = 1.54178 Å, step size of 0.02 and scan step time of 0.80 s). Furthermore, FT-IR patterns were recorded using a MATTSON IR-5000S spectrophotometer with a total reflectance diminished by a diamond to monitor the functional groups in the structure (FT-DATR in wavenumber ranging from 500 to 4000 cm. corrtest CS350 was used for the electrochemical analysis of the catalysts as-produced, and the obtained data was fitted using CS workstation software.

2.5. Electrochemical Performances

The typical three-electrode setup was equipped with Ag/AgCl (KCl, saturated) and auxiliary electrodes and a Pt sheet as reference, respectively. GCE (3 mm) is fully covered by the material attained. The fabrication procedure of GCE for the detection of the three biomolecules were tested by CV, EIS and SWASV techniques. Typically, in an Eppendorf tube with 250 mL of 100% ethanol including 50 mL of 5 wt% Nafion, 5 mg of each electrocatalyst is sonicated. Thereafter, a black homogeneous slurry was obtained by dispersion in ultrasonic for 30 min. A GCE that had been thoroughly cleaned and dried was covered with 10 μL of the homogenous mixture. CV experiments were investigated at a scan rate with a potential range of −0.2 to 0.6 V. SWASV profiles were conducted at initial and final potentials of −1.1 and 0.8 V, respectively, 50 mV pulse height, 5 mV step height, 4 Hz frequency and a scan rate of 20 mV s^{-1}. Chronoamperometry is applied with potential -1.1 duration 180s.

3. Results and Discussion

3.1. Material Characterization

Figure 1 shows the powder X-ray diffraction (PXRD) patterns of graphene oxide, unmodified, and modified graphene[20]. The XRD patterns of graphite compared to graphene oxide exhibited an interlayer spacing of 0.77 nm, which is higher than that of graphite flakes owing to the intercalated water molecules, and oxygenated functional groups

that formed from its chemical oxidation. Alternatively put, graphene oxide is graphene that has been heavily covered in hydroxyl and other groups [21]. The XRD peak of GO at 2 θ = 12° is reduced by eliminating these groups from the graphene sheet's surface. This disappearance is proof that graphene was created. The characteristic graphite diffraction peak broadens because of the shortrange order in stacked stacks of graphene. The modified graphene XRD peak is almost moved to the lower angles, occurring at 2 θ = 24°, or an interlayer separation of 0.37 nm in addition to duplicate the intensity of this peak. The remaining minute quantity of residual functional groups with oxygen or other structural defects are the cause of this movement in the XRD pattern [22, 23]. The appearance of the new local isatin-graphene phase may indicate that a structural chemical process taking place between graphene's free electrons and those in isatin resulted in the formation of a chemical bond and a new crystalline phase., is one explanation for this change [24]. FTIR spectroscopy is utilized to investigate the functional groups of GO surface that have undergone chemical modification. Figure 1b's FTIR spectrum of GO shows absorption peaks at wavenumbers of 3406.5, 1737.04, 1205.2, and 1620 cm-1, respectively, that correspond to the stretching of hydroxyl (OH), carbonyl (C=O), epoxy (C-O), and aromatic (C=C), as shown in Figure 3 While Isatin's regular bands serve as functional groups. The stretching vibration of the NH2 group is detected as a broad band between 3200 and 3600 cm^{1}. at 1715 cm^{-1} point out stretching vibration of NH-C-O functional group. A new band at 1533 $cm^{-1}$was generated that is attributed to C=N vibrations characteristic of imine

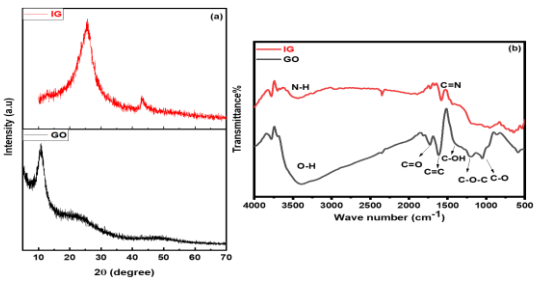

Fig.1 (a) XRD patterns of graphene oxide and modified graphene. (b) FT-IR spectra of graphene oxide (GO) and modified graphene.

SEM image of the ISG at different magnifications are shown in Figure (2) that displays the well- defined morphology of nanosheets. ISG is clearly observed as exfoliate structures with wrinkled forms.

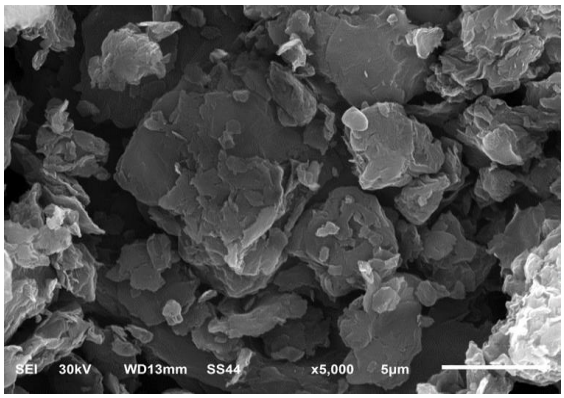

Fig. 2. SEM images of modified graphene.

3.2. Electrochemical performance of Graphene and modified graphene.

In solution of 0.1 M KCl, we dissolved of an equivalent weight 1.0 mM $[Fe(CN)_6]^{3-/4-}$, the electrochemical characteristics of the ISG/GCE were examined by CV and EIS. For comparison, the EIS plots and CV curves of the bare GCE, GO/ GCE, and ISG/GCE were also recorded. Using a pristine GCE, a pair of distinct redox peaks $[Fe(CN)_6]^{3-/4-}$ may be shown, as shown in Fig. 3a. On the GO/GCE, however, the currents of redox peak $[Fe(CN)_6]^{3-/4-}$increasing gradually, while the ISG /GCE The peak potential difference (E_p) is greatly decreased, and $[Fe(CN)6]^{3-/4-}$ current signal is enhanced. According to the results, the ISG/GCE performs more electrochemically than the GO/GCE. This might be explained by the Isatin's good interaction and even distribution throughout the RGO nanosheets. One benefit of having good contact between the two is that the hybrid material's conductivity is increased.

Moreover, EIS measurement was tested to further confirm the electron chemical performance of as-synthesized material. The EIS measurements of the electrode composites were studied with a sweeping frequency in the range between 0.01 and 10^5 Hz in 1.0 mM $[Fe(CN)_6]^{3-/4-}$ as the background electrolyte. The low and high-frequency portions of Nyquist diagrams for AC impedance are each represented by a straight line and a semicircle, respectively, as depicted in Fig.3 b. The straight-line part was ascribed to the diffusion

process, whereas the semicircle section was attributed to an electron transfer-limited approach. The intercept at the X-axis in the corresponding circuit diagram is represented by R_s, the resistance of electron transfer is denoted by R_{ct} and the Warbury impedance (W) influences how quickly electrolyte ions diffuse through electrode material in the low-frequency domain and is shown by the slope of a line [25-29]. The electron transfer resistance (R_{ct}) is represented by the semicircle's diameter in the EIS profiles. The following sequence represents the R_{ct} change: bare GCE > GO > ISG. These results illustrated that ISG can accelerate the charge transfer at the interface between $[Fe(CN)_6]^{3-/4-}$ and fabricated electrode in an electrochemical cell. We measured each metal ion's concentration individually and then recorded its SWASV responses to confirm the reliability of a ratiometric electrochemical method for the simultaneous determination of several ions of heavy metals. In Fig. 4, Metal ions concentration Cu^{2+}, Hg^{2+}, Pb^{2+} and Cd^{2+} ranges from 5 µM to 20 µM. As the concentration increases, the metal ions' peak currents gradually rise. This demonstrates the viability of the sensing platform based on the ISG for the simultaneous determine of C d^{2+}, Cu^{2+}, Hg^{2+} and Pb^{2+}.

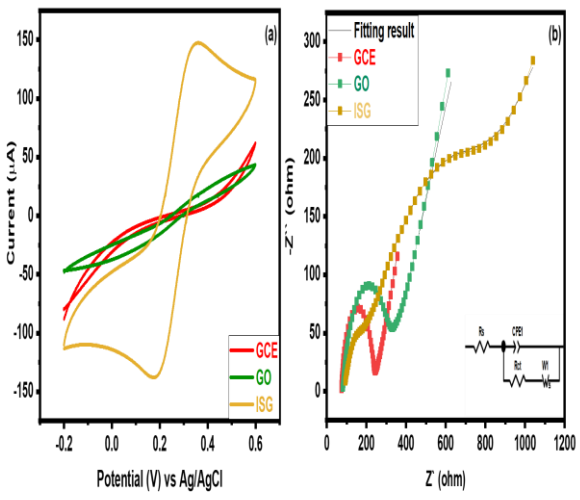

Fig.3. (A) Cyclic voltammograms and (B) Nyqust plots of bare GCE, graphene oxide (GO) and modified

graphene.in 0.1 M KCl that contain 1.0 Mm $[Fe(CN)6]^{3-/4-}$. The magnification of the Nyquist plots of several electrodes are shown in the inset.

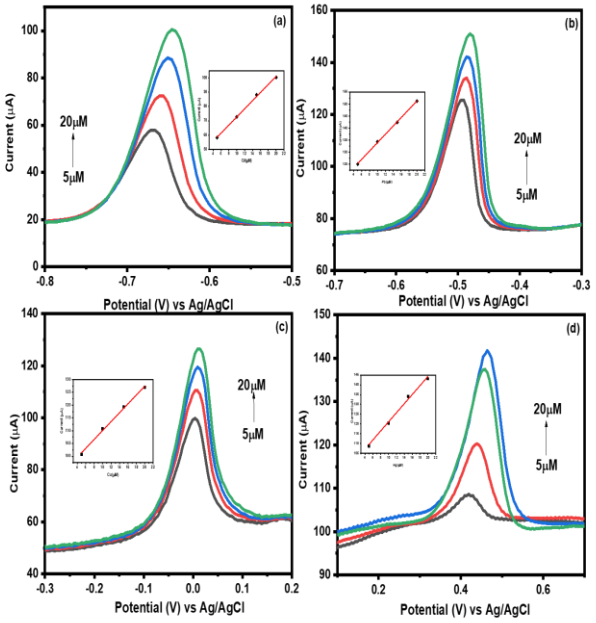

Fig.4: SWASV (the inset is the calibration curve) of different concentrations of an individual (a) $Cd^{2+,}$ (b) Pb^{2+}, (c) Cu^{2+} and Hg^{2+} (5- 20 µM) in 0.1 M HAc-NaAc buffer solution (PH= 5).

3.3. Optimization of the experimental conditions.

Various experimental parameters, including accumulation potential and accumulation time, were controlled to get the optimal performance of the sensing platform.

On the electrochemical signals of Cd^{2+}, Pb^{2+}, Cu^{2+}, and Hg^{2+}, the accumulation effects of both potential and time were estimated. According to Figure 5a, when the agglomeration potential was changed from 1.0 V to 1.1 V, the currents of these peaks gradually increased. The reduction of the four ions on the electrode surface is facilitated by the accumulation potential's negative shift, which causes this phenomenon to occur. The four heavy metal ions' shifts in reaction currents, however, exhibit distinct trends at more negative potentials[30]. Peak currents for Pb^{2+}, Cu^{2+}, and Cd^{2+} appear at 1.1 V and 1.2 V, respectively, each reaching their maximum values. Taken into consideration the possibility of reaction of hydrogen evolution occurring at a greater negative voltage.

Thus, the simultaneous determination of the proposed was performed at -1.1 V. In Fig. 5b, the accumulation time optimization's results are displayed. As shown, the currents of peak of

Cu^{2+}, Hg^{2+}, Pb^{2+}, and Cd^{2+} rose significantly with the increase of the accumulation time. From 60 s to 180 s, respectively, the four heavy metal ions' maximum peak currents were measured. It was suggested that setting 180 s as the accumulation period for the detection of ions would result in a stable peak with greater sensitivity and quicker analysis time.

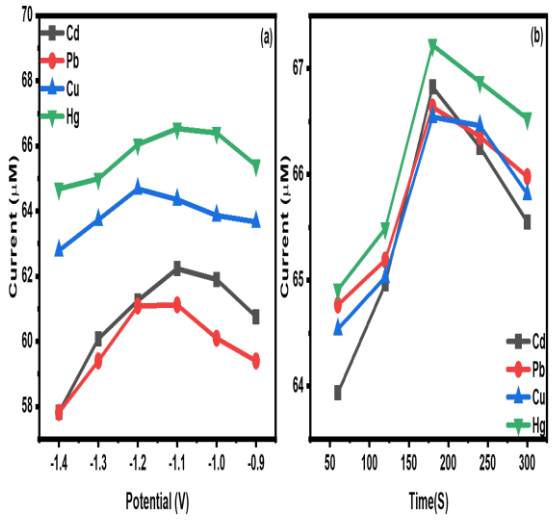

Fig. 5. Optimization of experimental conditions. Influence of (a) agglomeration potential, and (b) agglomeration time on the stripping peak current of Cu^{2+}, Pb^{2+}, Cd^{2+} and Hg^{2+} on the ISG/GCE.

3.4. Simultaneous investigation of Hg^{2+}, Pb^{2+}, Cu^{2+} and Cd^{2+}

The simultaneous detection of different HMIs with high sensitivity and accuracy presents a significant difficulty owing to the competing adsorption between the HMIs and their varying affinities with carbon materials. It was achieved in this study to detect Pb^{2+}, Cd^{2+}, Cu^{2+}, and Hg^{2+} simultaneously on the ISG/GCE. To evaluate the SWASV current signals of Pb^{2+}, Hg^{2+}, Cu^{2+}, and Cd^{2+} under optimal conditions, the concentrations are simultaneously increased from 5 M to 15 M at the potential interval between -1.0 V and 0.8 V. From Figure 6, as concentrations increase, the currents of peak of the four ions of metal steadily increase, observed a weak peak at approximately - 0.41 V between the Cu^{2+} and Pb^{2+} signals which resulting from the synthesis of intermetallic Pb-Cu complex during the process of deposition [31]. By simultaneously detecting solutions containing Cd^{2+}, Hg^{2+}, Cu^{2+}, and Pb^{2+}, the effectiveness of the suggested sensor was determined. As can be seen, there is no interference between the electrochemical signals for each metal ion.

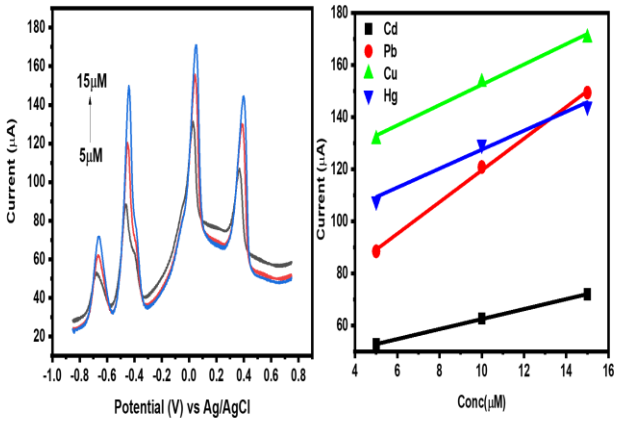

Fig. 6 (a) SWASV response of the ISG/GCE after the addition of different concentrations of Hg^{2+}, Cu^{2+}, $Pb^{2+}$and Cd^{2+} (from 5 μM to 15 μM) in a buffer solution at PH 5 and (b) calibration curves of the metal ions.

5. Conclusion

In this study, a novel functionalized graphene using isatin as a chelating agent was synthesized. Additionally, a platform for ratiometric electrochemical sensing based on the carbon material has been designed for the detection of several heavy metal ions. Graphene, one of the components of the composite, has a significant specific surface area, which is helpful for increasing the diffusion and preconcentration of metal ions. The chelator (isatin) not only increases the material's conductivity but also provided as the internal reference for the development of ratiometric detection, which enhances the material's electrochemical characteristics even more. Due to the sensing platform's distinctive structural features and strong electrochemical performance, simultaneous monitor of Cd^{2+}, Cu^{2+}, Hg^{2+}, and Pb^{2+} with great convenience, sensitivity, and reliability has been made possible. According to estimates, the ratiometric electrochemical sensor's LODs for Cd^{2+}, Pb^{2+}, Cu^{2+}, and Hg^{2+} were 1.37 μM, 0.5 μM, 1 μM, and 1.35 μM, respectively. With these benefits, a sensitive, straightforward, and reliability electrochemical sensor is considered as a promising material for environmental applications with a large scale.

4. References

1. S. Razzaque, K. Wang, I. Hussain, B. Tan, (2019) Facile synthesis of hypercrosslinked hollow microporous organic capsules for electrochemical sensing of cuii ions, *Chem. Eur. J*, **25** 548-555.
2. B.L. Vallee, D.D. Ulmer, (1972) Biochemical effects of mercury, cadmium, and lead, Annu Rev Biochem, **41** 91-128.
3. M.J. Hynes, B. Jonson, (1997) Lead, glass and the environment, Chem Soc Rev, **26** 133.
4. L. Jarup, (2003) Hazards of heavy metal contamination, Br Med Bull, **68** 167-182.
5. M.D. Esteban-Vasallo, N. Aragonés, M. Pollan, G. López-Abente, B. Perez-Gomez, (2012) Mercury, cadmium, and lead levels in human placenta: a systematic review, Environ Health Perspect, **120** 1369-1377.
6. Y. Lu, X. Liang, J. Xu, Z. Zhao, G. Tian, (2018) Synthesis of CuZrO3 nanocomposites/graphene and their application in modified electrodes for the co-detection of trace Pb(II) and Cd(II), Sensors and Actuators B: Chemical, 273 1146-1155.
7. K. Khatoon, A. Malik, (2021) Cyto-genotoxic potential of petroleum refinery wastewater mixed with domestic sewage used for irrigation of food crops in the vicinity of an oil refinery, Heliyon, **7** e08116.
8. J.B. Willis, (1962) Determination of lead and other heavy metals in urine by atomic absorption spectroscopy, Anal Chem, **34** 614-617.
9. P. Schramel, I. Wendler, J. Angerer, (1997) The determination of metals (antimony, bismuth, lead, cadmium, mercury, palladium, platinum, tellurium, thallium, tin and tungsten) in urine samples by inductively coupled plasma-mass spectrometry, Int Arch Occup Environ Health, **69** 219-223.
10. H. Guo, D. Wang, J. Chen, W. Weng, M. Huang, Z. Zheng, (2016) Simple fabrication of flake-like NH 2 -MIL-53(Cr) and its application as an electrochemical sensor for the detection of Pb 2+, *Chemical Engineering Journal*, **289** 479-485.
11. A. Yuan, X. Wu, X. Li, C. Hao, C. Xu, H. (2019) Kuang, Au@gap@AuAg Nanorod Side-by-Side Assemblies for Ultrasensitive SERS Detection of Mercury and its Transformation, Small, e1901958.
12. X. Fang, X. Chen, Y. Liu, Q. Li, Z. Zeng, T. Maiyalagan, S. Mao, (2019) Nanocomposites of Zr(IV)-Based Metal–Organic Frameworks and Reduced Graphene Oxide for Electrochemically Sensing Ciprofloxacin in Water, ACS Appl. Nano Mater., **2** 2367-2376.
13. R. Aswathi, K.Y. Sandhya, (2018) Ultrasensitive and selective electrochemical sensing of Hg(ii) ions in normal and sea water using solvent exfoliated MoS2 : affinity matters, *J. Mater. Chem. A*, **6** 14602-14613.
14. L. Xiao, H. Xu, S. Zhou, T. Song, H. Wang, S. Li, W. Gan, Q. Yuan, (2014) Simultaneous detection of Cd(II) and Pb(II) by differential pulse anodic stripping voltammetry at a nitrogen-doped microporous carbon/Nafion/bismuth-film electrode, Electrochim Acta, **143** 143-151.
15. K.A. Mahmoud, H.-B. Kraatz, A (2007) bioorganometallic approach for the electrochemical detection of proteins: a study on the interaction of ferrocene-peptide conjugates with papain in solution and on Au surfaces, *Chem. Eur. J*, **13** 5885-5895.
16. Y. Zhu, S. Murali, W. Cai, X. Li, J.W. Suk, J.R. Potts, R.S. Ruoff, (2010) Graphene and graphene oxide: synthesis, properties, and applications, Adv Mater, **22** 3906-3924.
17. M. Pumera, A. Ambrosi, A. Bonanni, E.L.K. Chng, H.L. Poh, (2010) Graphene for electrochemical sensing and biosensing, TrAC Trends in Analytical Chemistry, **29** 954-965.
18. C. Shan, H. Yang, D. Han, Q. Zhang, A. Ivaska, L. Niu, (2010) Graphene/AuNPs/chitosan nanocomposites film for glucose biosensing, Biosens Bioelectron, **25** 1070-1074.
19. D.A. Kospa, A.I. Ahmed, S.E. Samra, A.A. Ibrahim, (2021) High efficiency

solar desalination and dye retention of plasmonic/reduced graphene oxide based copper oxide nanocomposites, RSC Adv, **11** 15184-15194.
20. S. Thakur, N. Karak (2012), Green reduction of graphene oxide by aqueous phytoextracts, Carbon N Y, **50** 5331-5339.
21. D.C. Elias, R.R. Nair, T.M.G. Mohiuddin, S.V. Morozov, P. Blake, M.P. Halsall, A.C. Ferrari, D.W. Boukhvalov, M.I. Katsnelson, A.K. Geim, K.S(2009). Novoselov, Control of graphene's properties by reversible hydrogenation: evidence for graphane, Science, **323** 610-613.
22. S. Park, J. An, I. Jung, R.D. Piner, S.J. An, X. Li, A. Velamakanni, R.S. (2009) Ruoff, Colloidal suspensions of highly reduced graphene oxide in a wide variety of organic solvents, Nano Lett, **9** 1593-1597.
23. D. Li, M.B. Müller, S. Gilje, R.B. Kaner, G.G. Wallace, (2008) Processable aqueous dispersions of graphene nanosheets, Nat Nanotechnol, **3** 101-105.
24. J.R.N. Santos, D.S.S. Viégas, I.C.B. Alves, A.D. Rabelo, W.M. Costa, E.P. Marques, L. Zhang, J. Zhang, A.L.B. Marques, (2019) Reduced Graphene Oxide-Supported Nickel(II)-Bis(1,10-Phenanthroline) Complex as a Highly Active Electrocatalyst for Ethanol Oxidation Reaction, Electrocatalysis, **10** 560-572.
25. C. Hu, J. Xu, Z. Lu, C. Cao, Y. Wang, (2021) Core-shell structured ZIF-7@ZIF-67 with high electrochemical performance for all-solid-state asymmetric supercapacitor, *Int. J. Hydrog. Energy*, **46** 32149-32160.
26. C.V.V.M. Gopi, R. Vinodh, S. Sambasivam, I.M. Obaidat, S. Singh, H.-J. Kim ,(2020) Co9S8-Ni3S2/CuMn2O4-NiMn2O4 and MnFe2O4-ZnFe2O4/graphene as binder-free cathode and anode materials for high energy density supercapacitors, *Chem. Eng. J.*, **381**.
27. Z. Yuan, H. Wang, J. Shen, P. Ye, J. Ning, Y. Zhong, Y. Hu, (2020) Hierarchical Cu2S@NiCo-LDH double-shelled nanotube arrays with enhanced electrochemical performance for hybrid supercapacitors, *J. Mater. Chem. A*, **8** 22163-22174.
28. K. Zheng, G. Li, C. Xu, (2019) Advanced battery-supercapacitor hybrid device based on Co/Ni-ZIFs-derived NiCo2S4 ultrathin nanosheets electrode with high performance, Appl. Surf. Sci., **490** 137-144.
29. X. Meng, M. Feng, H. Zhang, Z. Ma, C. Zhang, (2017) Solvothermal synthesis of cobalt/nickel layered double hydroxides for energy storage devices, *J. Alloys Compd*., **695** 3522-3529.
30. X. Wang, Y. Qi, Y. Shen, Y. Yuan, L. Zhang, C. Zhang, Y. Sun, A (2020) ratiometric electrochemical sensor for simultaneous detection of multiple heavy metal ions based on ferrocene-functionalized metal-organic framework, Sensors and Actuators B: Chemical, **310** 127756.
31. W. Xiong, L. Zhou, S. Liu, (2016) Development of gold-doped carbon foams as a sensitive electrochemical sensor for simultaneous determination of Pb (II) and Cu (II), *Chemical Engineering Journal*, **284** 650-656.